Thermo-fluid dynamics and corrosion analysis of a self cooled lead lithium blanket for the HiPER reactor

2015 Nucl. Fusion 55 093003

(http://iopscience.iop.org/0029-5515/55/9/093003)

OPEN ACCESS
IOP Publishing | International Atomic Energy Agency
Nuclear Fusion
Nucl. Fusion **55** (2015) 093003 (12pp)
doi:10.1088/0029-5515/55/9/093003

Thermo-fluid dynamics and corrosion analysis of a self cooled lead lithium blanket for the HiPER reactor

R. Juárez[1], C. Zanzi[2], J. Hernández[2] and J. Sanz[1]

[1] Departamento de Ingeniería Energética, UNED, Juan del Rosal 12, E-28040 Madrid, Spain
[2] Departamento de Mecánica, UNED, Juan del Rosal 12, E-28040 Madrid, Spain

E-mail: czanzi@ind.uned.es

Received 1 December 2014, revised 7 May 2015
Accepted for publication 27 May 2015
Published 30 July 2015

Abstract

The HiPER reactor is the HiPER project phase devoted to power production. To reach a preliminary reactor design, tritium breeding schemes need to be adapted to the HiPER project technologies selection: direct drive ignition, 150 MJ/shot × 10 Hz of power released through fusion reactions, and the dry first wall scheme. In this paper we address the main challenge of the HiPER EUROFER-based self cooled lead lithium blanket, which is related to the corrosive behavior of Pb–15.7Li in contact with EUROFER. We evaluate the cooling and corrosion behavior of the so-called separated first wall blanket (SFWB) configuration by performing thermo-fluid dynamics simulations using a large eddy simulation approach. Despite the expected improvement over the integrated first wall blanket, we still find an unsatisfactory cooling performance, expressed as a low outlet Pb–15.7Li temperature plus too high corrosion rates derived from local Pb–15.7Li high temperature and velocity, which can mainly be attributed to the geometry of the channels. Nevertheless, the analysis allowed us to devise future modifications of the SFWB to overcome the limitations found with the present design.

Keywords: blanket design, EUROFER-based self cooled lead lithium, HiPER reactor, lead lithium corrosion rates, large eddy simulation, CFD, forced convection

(Some figures may appear in colour only in the online journal)

1. Introduction

The European High Power Laser Energy Research (HiPER) facility [1], dedicated to demonstrating laser driven fusion as a future energy source, is divided into two phases: HiPER engineering and HiPER reactor. This division foresees HiPER reactor conceived to be the power producing extension of the technologies developed during the HiPER engineering phase [2–6]. It would be a 150 MJ/shot × 10 Hz inertial fusion energy (IFE) reactor based on direct drive ignition [7] and the dry wall concept [8, 9]. Once the ignition scheme and first wall (FW) concept are fixed, it is necessary to advance in the proposal of reaction chamber characteristics: tritium breeding blanket and vacuum vessel systems. On the basis of previous neutronics [10] and power cycle studies [11], a self cooled lead lithium (SCLL) with EUROFER structure as the breeding blanket was approved by the HiPER team for exploration [1, 12].

The large majority of lead-lithium eutectic (Pb–Li) blankets have been designed for magnetic fusion energy (MFE) reactors, where Pb–Li is in direct contact with electric conductors (steel) under a high magnetic field. Under these conditions, large velocities of Pb–Li produce high pressure drops that cause high mechanical stress [13]. Consequently, in MFE, the fast flowing Pb–Li inside the blanket requires aggressive technological solutions, mainly based on the use of SiC. In increasing order of technological complexity, previous MFE

Pb–Li blanket concepts were: water cooled lead lithium (WCLL) [14], helium cooled lead lithium (HCLL) [15], dual coolant lead lithium (DCLL) [16] and self cooled lead lithium (SCLL) [17].

The development roadmap for Pb–Li breeders in MFE, relying on the development of SiC and SiC_f/SiC as structural material, has been naturally translated into the inertial confinement fusion (ICF) concepts, as considered in the high average power laser (HAPL) reactor, using the DCLL approach [18]. However, since there are no large magnetic fields in the reaction chamber of ICF reactors, Pb–Li may flow with no *a priori* velocity limitation, with no need of SiC or any other electrical insulator. This brings the possibility of exploring SCLL schemes using EUROFER as the structural material. In a EUROFER-based SCLL blanket, with no flow channel inserts or SiC components, the temperature operation window for Pb–Li could be equivalent to that of WCLL or HCLL blankets: 350 °C–500 °C. This scheme, only viable for ICF reactors, presents two evident advantages: (i) it does not require complex hollowed blanket walls for heat exchange inside the reaction chamber, and (ii) EUROFER is a much more mature material than SiC, implying a technological risk comparable to that of the WCLL or HCLL MFE blankets, considered to be short-term technologies. Furthermore, there is a final advantage of the SCLL scheme over the rest: the high Pb–Li velocity leads to very low concentrations and partial pressures of tritium and other gaseous radioactive threatening isotopes (e.g. ^{210}Po and ^{203}Hg), with evident safety advantages [10]. In summary, the EUROFER-based SCLL blanket is simpler than WCLL and HCLL blankets in terms of constructability and design, and presents safety advantages, while all of them show comparable technological risks.

Despite the above, there is in fact a process likely limiting the Pb–Li velocity inside the EUROFER-based SCLL blanket: the corrosive behavior of Pb–Li in contact with EUROFER, which depends on its temperature and velocity. This issue has been characterised before in laboratory experiments [17, 19, 20], and it is still under study. However, as MFE DCLL and SCLL blankets considered SiC–hot Pb–Li interfaces, instead of EUROFER–hot Pb–Li interfaces, there is not currently a quantification of the corrosion challenge for a specific EUROFER-based SCLL design. This situation, which represents a knowledge gap of a design driver and a source of uncertainties for the viability of the EUROFER-based SCLL blanket concept, constitutes the main subject of the paper. If the risk associated with the corrosion challenge is found to be low, assumable, or even reducible with re-design or short-term materials, EUROFER-based SCLL would be a strong candidate for HiPER reactor or any other ICF reactor in the short-term scale.

Thus, for the initial EUROFER-based SCLL proposal for the HiPER reactor [1, 10–12], we study in this paper both the cooling performance and the corrosion issue. Cooling performance is addressed in terms of maximum local temperatures (limited to 550 °C, EUROFER creep rupture temperature) and outlet Pb–Li mean temperature (desirable to be around 450 °C, for power cycle efficiency [11]). The corrosion issue is addressed in terms of maximum local corrosion rates, which is limited to 200 μm yr^{-1}. To carry out this study, both computational neutronics and thermo-fluid dynamics simulations are used to properly characterise the nuclear heat deposition and extraction.

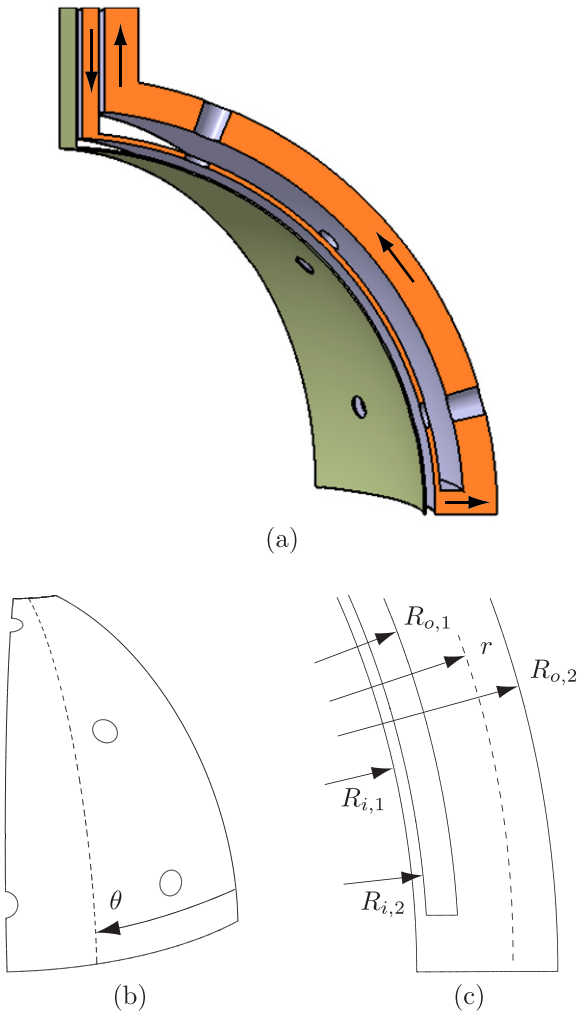

Figure 1. (*a*) Schematic representation of a 45° module of the breeding blanket, showing the first wall (colored green) and Pb–15.7Li circulation through the inner and outer channels. (*b*) Spherical section of the blanket module and azimuthal coordinate, θ. (*c*) Meridian section of the blanket module and radii of the channel walls.

1.1. Self cooled lead lithium blanket of HiPER

The SCLL breeding blanket (BB) configuration with a 15.7% of atomic content of lithium in eutectic, proposed in previous works for the initial design of the HiPER project, is adopted here [10]. Figure 1 shows the geometry of the blanket, which consists of 45° modules that account for the laser beams symmetry. Each module consists of a downflow inner channel, with inner and outer internal walls of radii $R_{i,1}$ = 6.51 m and $R_{i,2}$ = 6.59 m, and an upflow outer channel, with inner and outer internal walls of radii $R_{o,1}$ = 6.81 m and $R_{o,2}$ = 7.51 m. In each hemisphere of the blanket there are 24 laser beam penetration holes, uniformly distributed on three parallels of latitudes 69.77° (4 holes), 42.97° (8 holes) and 15.05°

(12 holes). The lower 2nd and 3rd sets of holes have azimuthal offset angles, with respect to the uppermost, of 23.36° and 29.83°, respectively. The height of the transition region between the downflow and upflow channels is 40 cm.

There were two reasons for this BB modular division. The first one is its compatibility with laser beams arrangement symmetry, which requires the construction of only two different and mirrored modules, which is a fabrication advantage. The second and most important reason is related to the heat deposition and removal. Most of the energy deposited in the BB comes from the neutrons released upon ignitions. The neutrons will deposit their energy mainly in the Pb–15.7Li. The nuclear heat deposition rate decays exponentially with depth, so that a large fraction of the nuclear heat will be deposited in the first centimeters of the BB. This is taken into account in the design by setting a thin cooling channel close to the neutrons source, and an outer thicker channel (see figure 1). The Pb–15.7Li velocity in the inner channel will be significantly higher than that in the outer channel, as demanded by the heat deposition profile. In addition, the fast flowing Pb–15.7Li in the inner channel will be colder, while the hot Pb–15.7Li in the outer channel will move slower. Thus, this modular division is aimed at mitigating the corrosion issues by using a combination of a cold and fast flow through the inner channel and a hot and slow flow through the outer channel, avoiding the worst combination, from corrosion standpoint, of hot and fast Pb–15.7Li flow.

A design aspect that has to be defined affects the FW configuration. This component consists of a substrate and a coating. Normally, the FW substrate, which holds the coating, is made of EUROFER or other reduced activation ferritic/martensitic (RAFM) steel. In the dry wall IFE scheme, the operating conditions of the FW materials are very demanding [8, 9], especially for the FW coating. Ions and x-rays, carrying approximately the 25% (375 MW) of the power released upon ignition, are deposited in the first layers of material. On the assumption that satisfactory materials will eventually be developed, this power would have to be evacuated from the FW. The remaining 75% (1125 MW) of the power is carried by neutrons depositing their energy mostly in the rest of the breeding blanket. An initial and simple approach to SCLL blanket involves transferring the heat deposited in the FW to the flowing Pb–15.7Li, so that it is evacuated with the heat deposited in the rest of the blanket. However, since the energy deposited in the FW is not related with any tritium breeding (associated to neutron reactions with lithium), it is not strictly necessary to extract it with the breeder/coolant. Furthermore, this energy will contribute to increase the temperature of the coolant and the required circulation velocity of Pb–15.7Li, and thus the corrosion rate, with no advantage in terms of blanket performance (no extra tritium breeding ratio (TBR), no extra shielding). In addition, the FW component is exposed to degradation mechanisms different from those of the BB.

Therefore, in the present work we consider a Separated First Wall Blanket (SFWB) configuration in which FW and BB are physically independent components, so that the first wall could be cooled with helium and the BB maintains the self-cooled scheme, in which the Pb–15.7Li evacuates the 100% of the energy deposited in it. This idea of a self cooled lead lithium blanket with helium-cooled FW was addressed previously in [17]. It was shown in [10] that the FW–BB decoupling could be made without compromising the blanket tritium breeding capabilities. The SFWB configuration was studied in [11] from the standpoint of power cycle efficiency. Assuming a helium Brayton cycle as the secondary loop for electric power production, a significant increase was found in the computed efficiency of the SFWB configuration over the integrated first wall blanket (IFWB) configuration when cooling the separated first wall with a helium branch from the secondary circuit. However, although the main goal of the SFWB configuration is to mitigate the corrosion problems derived from a fast flowing Pb–15.7Li in direct contact with EUROFER [13, 17, 19–21], the fluid dynamics behaviour of the SCLL reference design proposed in [10] has not been evaluated yet.

In this work, on the basis that SFWB will perform better than IFWB, as it is reasonable to expect, we compute the coolant/breeder heat extraction performance for the SFWB configuration (IFWB will only be studied if significant advantages were found in other aspects related to reactor operation, such as maintenance, safety, constructability, etc). In addition, the corrosion implications of the fast flowing Pb–15.7Li for this arrangement of the SCLL are addressed. We aim to devise further improvements of the proposed blanket/SCLL design, taking into account the results of the numerical simulations for several operational scenarios.

1.2. Design goals

The conceptual design of the SCLL blanket has to fulfill a serial of cooling requirements to guarantee the structural integrity and economic viability of the power plant. Intrinsically related to the cooling requirements, the serious challenge of the corrosion is also present. In this section, we justify the design requirements for the HiPER SCLL breeding blanket.

1.2.1. Cooling requirements. The proper cooling of the blanket requires the following two conditions:

- The maximum temperature of the interface between Pb–15.7Li and EUROFER inside the blanket should be less than 550 °C.
- The temperature of the Pb–15.7Li at the blanket outlet should be around 450 °C (assuming that the temperature at the inlet is 350 °C).

The first condition is derived from the EUROFER behavior. Above 550 °C the EUROFER is exposed to a degradation of its mechanical properties, mainly driven by creep rupture [22]. The second condition is found to be a compromise between the power cycle efficiency and the corrosion rates in the whole facility. Note that it is set on a conservative basis. In future designs, as the Pb–15.7Li corrosion issue is solved, the second requirement could be raised up to approximately 550 °C, similarly to WCLL and HCLL blankets. Future developments, like ODS-EUROFER [23, 24], anticorrosion coatings [25] and SiC_f/SiC [26] would allow to significantly raise this temperature.

1.2.2. Corrosion requirements. The materials compatibility issue is, together with the proper blanket cooling, the main scope of this paper. The fast flowing Pb–15.7Li, characteristic of the SCLL blanket, can have deep implications related to corrosion. The design target has been obtained by limiting to a 10% the total thickness reduction due to corrosion during the blanket lifetime, as proposed in [13]. Since the reference SCLL blanket for HiPER reactor has walls of 1 cm thickness, this 10% limit implies a corrosion design target of 200 μm yr^{-1} during the lifetime of the blanket modules, which is estimated in 5 years. Note that this target is valid only for the SCLL blanket reference design. If, for any reason, the wall thickness is modified (for structural requirements, for instance), the target should then be recalculated. It is worth mentioning that these estimations of corrosion restrictions are provisional and considered for conceptual design purposes only. As the conceptual design evolves, further studies will also have to consider additional corrosion limit drivers, as for example the deposition of eroded steel in the cold leg of the circuit [13].

2. Methodology

The two different methodologies used to carry out the three dimensional simulation of the nuclear heat deposition and extraction processes are presented in this section. We also explain the approach and assumptions made to compute the corrosion rates.

2.1. Nuclear heat deposition

The first step in the computation procedure is to develop a 3D model of the reaction chamber with CATIA [27]. Then, using MCAM [28], the resulting geometry of a BB module (45° of the northern hemisphere) is translated to a valid geometry input for MCNPX [29]. Thus, considering reflective boundary conditions and a shock ignition neutron spectra for the source [30], the nuclear heat deposition in a blanket module is computed using MCNPX and the cross sections libraries JEFF-3.1.1 [31]. Additionally, in order to visualise how the nuclear heat is deposited throughout the BB by neutrons, a mesh of $2.5 \times 2.5 \times 2.5$ cm^3 voxels is used. Note that this is not used in the heat extraction study, as both meshes are incompatible.

As shown in figure 1, the MCNPX geometry was initially separated into EUROFER and Pb–15.7Li cells. The Pb–15.7Li is in turn divided into 1 cm thick spherical shells. To compute the heat deposition, cell tallies are used for the four steel spherical shells and all the Pb–15.7Li cells. The cell-based results, which are extracted and appropriately formatted for CFD studies with C++ scripts, are the input for the heat extraction simulations.

2.2. Heat extraction

The numerical study of the Pb–15.7Li flow and cooling process in a 45° blanket module (figure 1(*a*)) is carried out using the general purpose CFD code FLUENT 6.3 [32], which is based on a finite volume discretization. The flow in the blanket is highly turbulent and three dimensional, with typical Reynolds numbers above 10^6. The physical properties of molten Pb–15.7Li are assumed to be given by the following equations: [33]

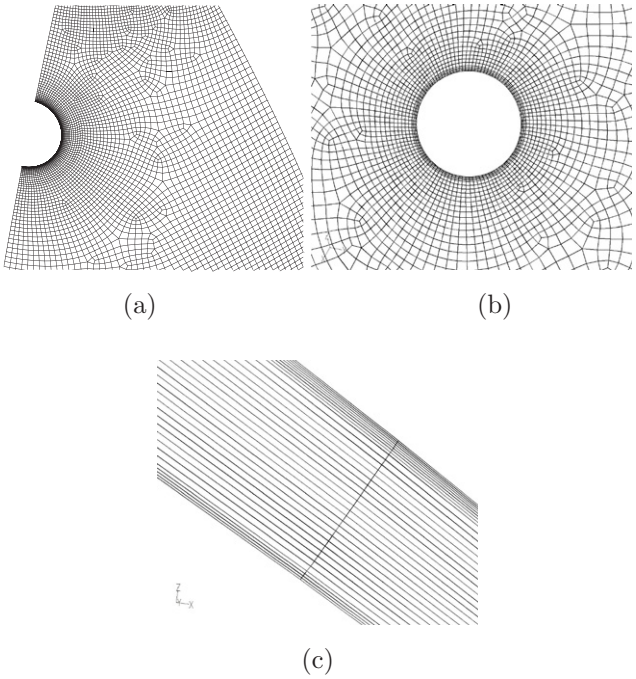

Figure 2. CFD mesh refinement details: (*a*) spherical walls, (*b*) beam laser penetration hole and (*c*) cross section of the inner channel.

$$\rho = 9990(1 - 1.680 \times 10^{-4}\, T), \tag{1}$$

$$c = 192.45 - 8.9487 \times 10^{-3}\, T, \tag{2}$$

$$\mu = 0.187 \exp\left[\frac{11.64}{R_u(T + 273.15)}\right], \tag{3}$$

$$k = 7.3008 + 1.96 \times 10^{-2}\, T, \tag{4}$$

where ρ is the density (expressed in kg m^{-3}), c the specific heat capacity (J kg^{-1} °C^{-1}), μ the viscosity (mPa s^{-1}), k the thermal conductivity (W m^{-1} °C^{-1}), T the temperature (°C) and R_u the universal gas constant (J mol^{-1} K^{-1}). According to [33], properties are determined in a sufficiently precise way in the operation temperature range considered in this work.

The governing conservation equations of mass, momentum and thermal energy are solved using a large eddy simulation approach for turbulence modeling, with a Smagorinsky-Lilly subgrid-scale model [34, 35] and a second-order implicit temporal discretization. The convective terms in the governing equations are discretised using a second order bounded central differencing scheme.

The non-uniform volumetric nuclear heat generation rate due to the deposition of neutrons energy in the Pb–15.7Li, calculated using MCNPX, is introduced as a source term in the energy equation. No-slip and uniform heat flux boundary conditions are imposed at all blanket walls and at each of the spherical walls delimiting the blanket channels, respectively. The heat flux at each of the four spherical walls is determined

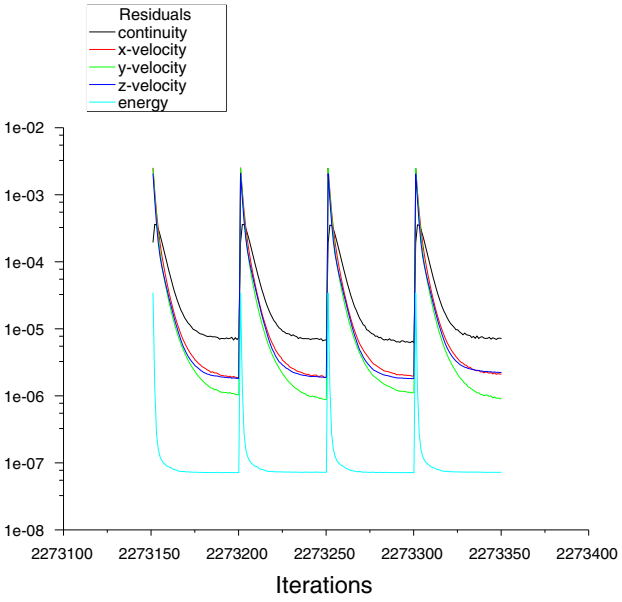

Figure 3. Typical evolution of residuals.

from the energy deposition rate in the EUROFER structure computed using MCNPX. All the other walls of the blanket are considered as adiabatic.

The finest computational mesh used in the simulations consists of about 3.5×10^6 hexahedral cells. The mesh is locally refined near the channel walls and around the laser penetration holes, where high gradients of flow quantities are expected. Figures 2(*a*)–(*c*) show, as an example, details of mesh refinement on one of the spherical walls of the blanket, around a beam laser penetration hole and in a cross section of the inner channel, respectively. The mesh refinement at the walls of the outer channel is similar to that shown in figure 2(*c*).

The sizes of the first layer of cells at the spherical walls and at the walls of the laser beam penetrations were kept equal to 2×10^{-5} and 2×10^{-4} m in the inner and outer channels, respectively, in order to obtain acceptable ranges of parameter y^+. We did not refine the mesh in the vicinity of the lateral walls of the channels and of the inlet and outlet pipes in order not to excessively increase the total number of cells, which otherwise would have multiplied by a factor of 2–3.

The typical time step used in the simulations is between 1.5 and 2 ms. After a maximum number of 50 iterations per time step, all residuals decreased at least two orders of magnitude and then remained low and almost constant. The scaled residuals defined in FLUENT [32] decreased to around 10^{-5}, 10^{-6} and 10^{-7} for the continuity, three components of momentum and energy equations, respectively (these values slightly increased with the volumetric flow rate of Pb–15.7Li through the blanket). Figure 3 shows, as an example, the evolution of residuals during four time steps of one of the simulations carried out.

Since the mesh generated with MCNPX for heat deposition is quite different from that used in FLUENT for the thermo-fluid dynamics simulation, we have coupled them using a C++ codification to export to FLUENT the distribution of the deposited nuclear heat calculated with MCNPX.

2.3. Corrosion

A description of the phases and phenomena involved in the complex corrosion process that may occur in the blanket can be found, for example, in [36–39]. In the present work, the transport of the steel elements dissolved from the blanket walls in the flowing liquid metal is not simulated numerically, and the corrosion process is treated in a simplified way. To estimate the corrosion rates produced by the Pb–15.7Li in the EUROFER of the SCLL reference design, we use Sannier's equation [19, 40] as initial approach for conceptual design activities:

$$\nu = 8 \times 10^9 \exp\left[\frac{-25\,690}{1.98\,T}\right] V^{0.875} d^{-0.125}, \qquad (5)$$

where ν is the corrosion rate expressed in μm yr^{-1}, T is the local temperature in K, d is the channel width (expressed in cm; $d = 8$ and 70 cm in the inner and outer channels, respectively), and V is the average value of the velocity magnitude of the fluid (in m s^{-1}) on an area of the cross-section of the channel with an azimuthal width of the order of the mean azimuthal size of the computational mesh cells on the whole cross section. According to [19, 40], using equation (5) is consistent with the assumption that the corrosion rate is controlled by the diffusion of the metallic elements of the blanket walls dissolved into the flowing Pb–Li. It is therefore assumed that the fluid velocity is low enough to produce mass transfer controlled corrosion and avoid high corrosion rates due to the effect of erosion [37, 38].

It should be pointed out that the above procedure for corrosion computation is an initial approximation. Given the complexity of the problem and the different sources of uncertainties involved, such as those associated with the determination of the saturation concentration [39], the dependence of the corrosion rate on the Pb-Li velocity [36] and the range of conditions of applicability of Sannier's equation, among others,

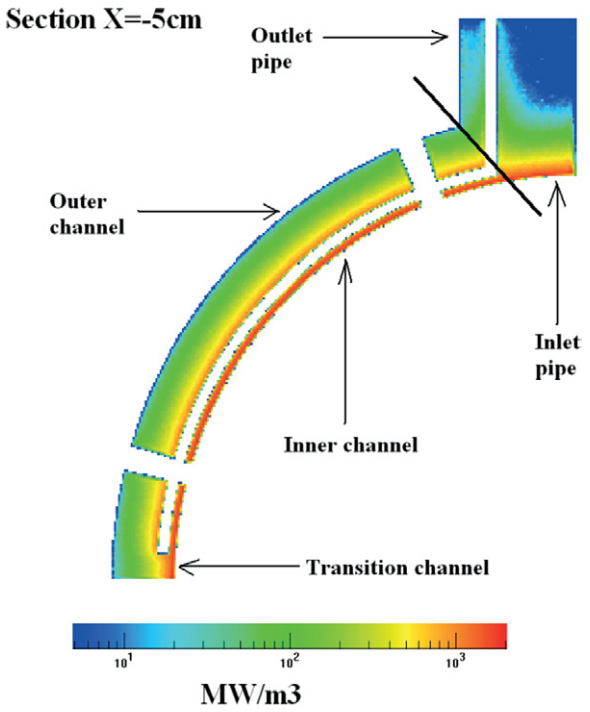

Figure 4. Distribution of the nuclear mean power deposited by neutrons in a blanket module.

we decided to postpone for a future work the simulation of the corrosion process in a fully coupled way with the thermo-fluid dynamics processes. Nevertheless, despite its simplicity, the approach used in the present work is expected to provide an accurate enough insight into the behavior of the proposed blanket design, and will allow us to obtain preliminary results that will be useful to devise a new design that overcomes the existing limitations, which could then be studied using a more advanced model for the flow-induced corrosion process.

3. Discussion of results

3.1. Nuclear heat deposition

As mentioned before, the power released upon ignitions is 150 MJ/shot × 10 Hz. The ions and the x-rays carry 375 MW, corresponding to the 25%, and the neutrons carry 1125 MW, the rest. The power carried by the ions and x-rays is fully deposited in the first microns of the first wall. On the other hand, as the neutrons are more penetrating in the matter, they pass through the first wall and deposit a large part of their energy in the blanket. In addition, neutrons induce exothermic reactions in the blanket structure and breeding. Then, although the neutrons carry 1125 MW, the total energy deposited in the blanket is 1322.5 MW. This withstands a blanket gain of $\eta_{\text{blanket}} = 1.175$.

Figure 4 shows the distribution of the neutron power deposition in the blanket module (EUROFER structure and Pb–15.7Li) for the IFWB configuration, which can conservatively be assumed to be similar for the SFWB arrangement. As expected, the nuclear heat deposition is significantly more intense in the first centimeters of the BB and exponentially decreases with thickness. Pb–15.7Li is conceived to re-generate tritium while extracting neutrons energy effectively. Table 1 shows the neutron power deposited in the different stretches of the blanket module. It is remarkable that, although the inner channel contains the 8.4% of the total Pb–15.7Li volume, it receives the 39.5% of the total neutron power deposition. The outer channel contains the 81.9% of Pb–15.7Li while it receives the 56.5% of the nuclear heat, which is a large contrast to the inner channel. This highlights the exponential decrease of heat deposition with depth, while it supports the BB modular division and ducts configuration with heat extraction criteria. In addition, it is confirmed that the EUROFER structure captures only about a 10% of the nuclear heat deposited in the BB, most of it in the inner channel walls.

Table 1. Total neutron mean power deposition in the BB (including breeder and structure), in the different stretches of a 45° blanket module.

Stretch	Neutron power Deposition [MW]	Pb–15.7Li Volume [m^3]
Inlet pipe	1.13	1.69
Inner channel	32.63	2.60
Transition channel	1.99	0.40
Outer channel	46.74	25.23
Outlet pipe	0.15	0.90
Total	82.65	30.8

3.2. CFD study of fluid flow and heat extraction

We present in this section the results obtained from the numerical simulation of the Pb–15.7Li flow and cooling process in the 45° blanket module, for the SFWB configuration and three different operational scenarios. In the three cases, the temperature of the Pb–15.7Li at the blanket inlet is $T_{\text{in}} = 350$ °C and the total nuclear heat deposition rate in the module is set equal to 82.65 MW. In all the simulations, a constant power released upon ignition is assumed, without taking into account the pulsed nature of the energy delivery and deposition. From the Pb-Li heat capacity values deduced from equations (1) and (2) for the range of operation temperatures and the data included in tables 1 and 2 for the inner channel, we can obtain an estimate of the increase in temperature during shots in the Pb-Li of the order of only 1 °C. Given the relatively high frequency and short duration of shots, and the large thermal inertia of the blanket, the amplitude of temperature change in the EUROFER will be even smaller. Therefore, the influence of the temperature oscillation on the corrosion rate is expected to be negligible. The heat deposited in the blanket structure is assumed to be transferred to the Pb–15.7Li through the spherical channel walls, with a uniform heat flux at each wall and the total heat transfer rate values indicated in table 2. The only parameter that varies in the simulations is the mass flow rate of Pb–15.7Li through the blanket module, $\dot{m}$, which is equal to 5993, 8557 and 11 410 kg s^{-1} in cases 1, 2 and 3, respectively. The selection of these $\dot{m}$ values was made using a trial-and-error procedure. The idea was to find a range of mass flow rates that could simultaneously satisfy the cooling and corrosion requirements.

Table 2. Total heat transfer rate at the blanket walls, due to neutron power deposition in the EUROFER structure.

	Heat transfer rate [MW]
Inner channel, inner wall	3.11
Inner channel, outer wall	3.11
Outer channel, inner wall	2.19
Outer channel, outer wall	0.188
Total	8.60

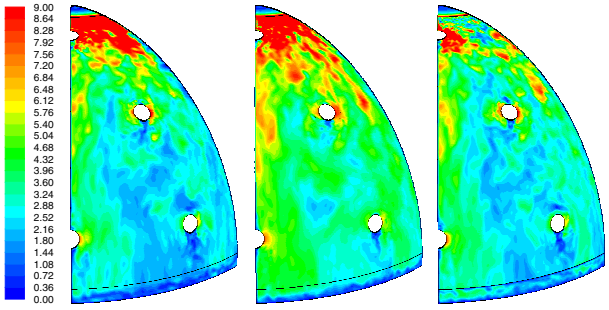

Figure 5. Velocity magnitude contours (m s^{-1}) at different spherical surfaces in the inner channel of the blanket module (Case 3).

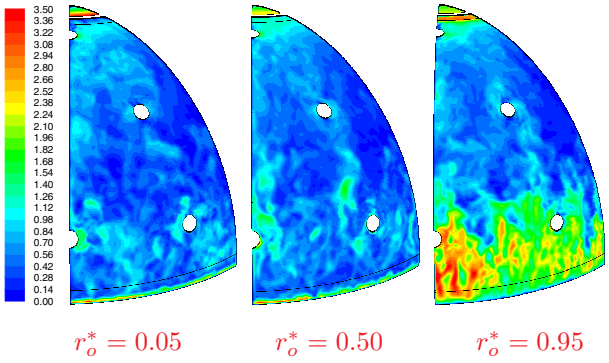

Figure 6. Velocity magnitude contours (m s^{-1}) at different spherical surfaces in the outer channel of the blanket module (Case 3).

Figures 5 and 6 show the results for the velocity magnitude contours within the inner and outer channels, respectively, on three different spherical surfaces bounded by the lateral channel walls, obtained at a given instant from the simulation of Case 3. The dimensionless radial coordinates of the surfaces are $r_i^* = (r - R_{i,1})/(R_{i,2} - R_{i,1}) = 0.05$, 0.50 and 0.95 in the inner channel and $r_o^* = (r - R_{o,1})/(R_{o,2} - R_{o,1}) = 0.05$, 0.50 and 0.95 in the outer channel, where r is the radial coordinate with origin at the center of the blanket (see figure 1(*c*)). Figure 7(*a*) shows the same type of results on three meridian planes of the blanket module, of dimensionless longitude angles $\theta^* = \theta/45° = 0.25$, 0.50 and 0.75 (the origin of θ is taken at the meridian plane through the lateral wall of the blanket where there are no laser penetration holes, as shown in figure 1(*b*)). A detail of the transition region between the inner and outer channels of figure 7(*a*) is shown in figure 8. It can be observed from all these figures that, besides the fluctuations associated to large-scale turbulence motions, there is also a notable nonuniformity in the fluid velocity in the whole blanket, which may affect the efficiency of the cooling process and lead to zones of high corrosion rates, as discussed below. The main factors that cause non-uniformity in the velocity distribution in the blanket are the variations in the channel cross-section area, the divergence of the inner channel, the presence of the laser penetration holes (which have an appreciably larger influence in the inner channel), and the recirculation effects occurring in the transition region between the two channels and at the entrance region to the blanket.

The small cross-section area at the top of the inner channel produces large velocities there, as shown in figure 5. Due to the recirculation produced by the change in direction of the flow entering the channel from the inlet pipe, the increase in velocity in this region is lower near the outer wall. As expected, the effect of the channel walls is more appreciable and large-scale turbulent motion on meridian planes is inhibited in the inner channel, which is much narrower than the outer one (see figures 7(*a*) and 8). It can be observed from figure 5 the non-uniform distribution of the fluid velocity at the bottom of the inner channel (more clearly shown in the proximity of the spherical walls, at $r_i^* = 0.05$ and 0.95), which can be attributed to the wakes of the two central penetration holes. At the bottom of the outer channel, downstream of the transition region between the inner and outer channels, there is a recirculation zone and larger velocities in the vicinity of the outer wall, as can be observed from the picture at the right of figure 6 ($r_o^* = 0.95$) and figures 7(*a*) and 8. A slightly uneven velocity distribution in the azimuthal direction persists at the bottom of the outer channel, which is more appreciable in the vicinity of the outer wall (see picture for $r_o^* = 0.95$ in figure 6). Note that the average velocity in this region is slightly higher in the half of the channel closer to the lateral wall where $\theta^* = 1$ (left side of the picture).

The temperature distributions shown in figures 9–11 are consistent with the velocity distributions described above. At the bottom of the inner channel, the average temperature varies slightly along the azimuthal direction, being larger around the middle meridian plane, what is consistent with the lower velocities found there. There is also a variation in the radial direction, so that the temperature is higher near the spherical walls (see figures 9 and 11), especially in the vicinity of the inner wall, where the fluid velocity is smaller (picture for $r_i^* = 0.05$ of figure 5). The slightly nonuniform distributions of the average temperature and velocity along the azimuthal direction persists at the entrance region to the outer channel, especially near the outer wall, as can be observed from figure 10. However, the effect of the flow conditions at the exit of the inner channel on the temperature distribution downstream in the outer channel seems to be small. It can be observed from figures 10 and 7(*b*) that there are notable temperature variations within the outer channel. Note that the average temperature obviously increases along the channel. Also note that the temperature is in general higher in the vicinity of the inner wall, what is mainly due to the higher heat flux from the wall (see table 2). The overall higher temperatures that are reached in the outer channel in the vicinity of the lateral wall at $\theta^* = 0$ (right side of pictures of figure 10) might

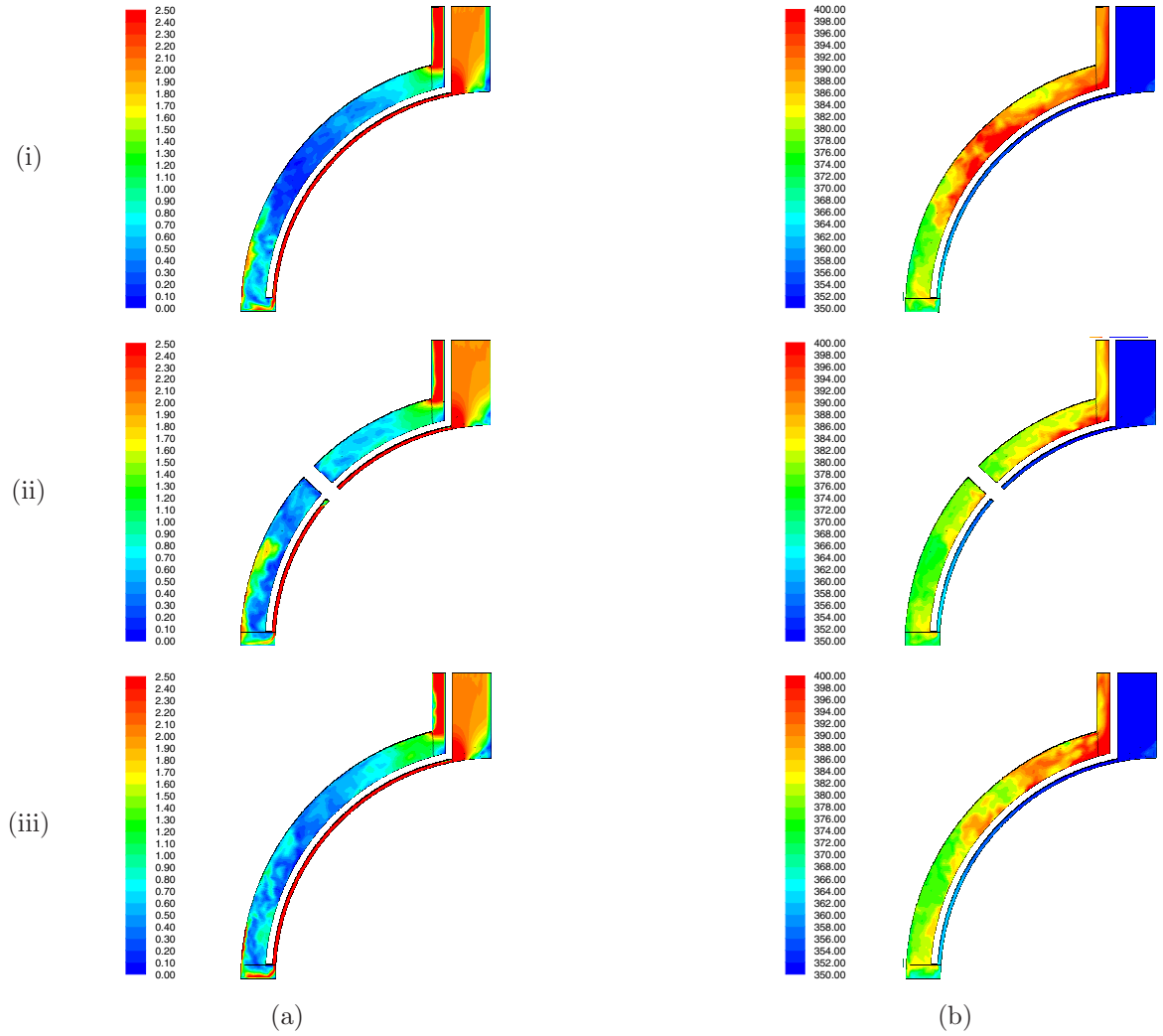

Figure 7. (*a*) Velocity magnitude contours (m s^{-1}) and (*b*) temperature contours (°C) at three meridian planes of the blanket module (Case 3): (i) $\theta^* = 0.25$; (ii) $\theta^* = 0.50$ and (iii) $\theta^* = 0.75$.

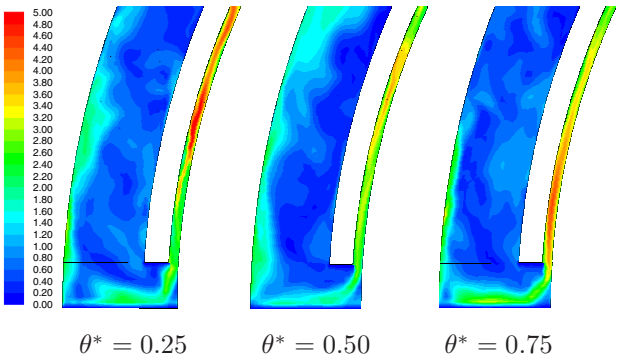

Figure 8. Detail of the velocity magnitude contours (m s^{-1}) in the transition region between the inner and outer channels in the pictures of figure 7(*a*).

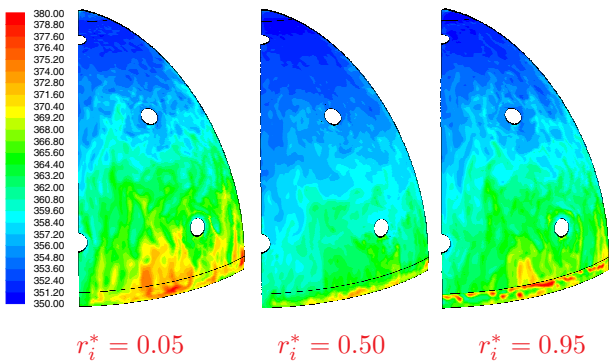

Figure 9. Temperature contours (°C) at different spherical surfaces in the inner channel of the blanket module (Case 3).

be related to the lower fluid velocity in this zone, which in turn seems to be partially caused by the presence of the laser penetration hole near the right bottom corner of the blanket ($\theta^* = 0$).

The overall flow pattern observed for cases 1 and 2 is qualitatively similar to that just described for Case 3, although the velocity magnitudes for the formers are obviously smaller due to the reduced mass flow rate of Pb–15.7Li.

Figure 12 shows the results for the distribution of the corrosion rate at the four spherical walls of the blanket module channels for the three operational scenarios considered. It can be observed that for cases 1 and 2 the highest corrosion rates occur at the inner wall of the end part of the outer channel,

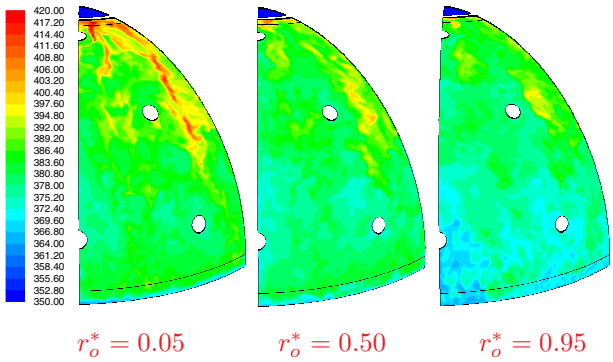

Figure 10. Temperature contours (°C) at different spherical surfaces in the outer channel of the blanket module (Case 3).

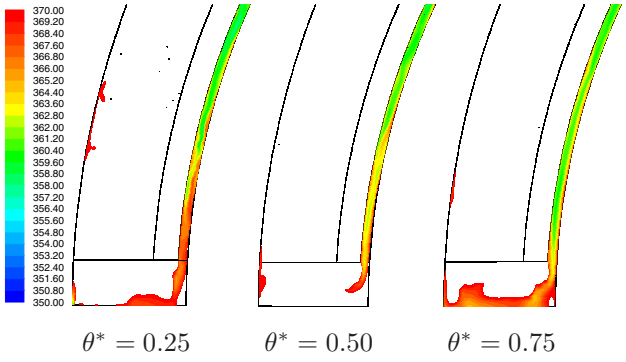

Figure 11. Detail of the temperature contours (°C) in the transition region between the inner and outer channels in pictures of figure 7(*b*).

where the increase in velocity due to the reduction of the cross-section area combines with the higher temperature of the Pb–15.7Li reached at the blanket outlet section as a result of cooling conditions worse than those of Case 3, especially for Case 1, for which a wide area of high corrosion rates is predicted. For Case 3, the highest corrosion rate values are predicted at the inner wall of the inner channel, around the penetration hole close to the inlet pipe, mainly because of the high velocity reached in that region. The main results obtained for cases 1, 2 and 3 are summarised in table 3, showing the maximum temperature reached in the Pb–15.7Li, T_{max}, the mean increase of temperature in the Pb–15.7Li between the inlet and outlet sections of the blanket, $T_{out} - T_{in}$, and the maximum corrosion rate (obtained from the distributions of velocity and temperature using (5)) reached in the channels spherical walls, ν_{max}. The first value of the corrosion rate shown for each case is the maximum value predicted in the whole domain. However, since these maximum values may be reached in a very localised area, a second value is also given in parenthesis, representing the minimum value of the corrosion rate reached at every point within an area of approximately 400 cm^2 around the point where the maximum corrosion rate is calculated.

Table 4 shows corrosion results obtained for cases 1, 2 and 3 in terms of volume of material removed and (in parenthesis) average corrosion rate values, both calculated over the four spherical walls of the blanket. For case 1 (lowest mass flow rate of Pb–15.7Li), due to the high temperatures reached in the region of the blanket close to the outlet pipe, the largest amount of material is removed from the inner wall of the outer channel, followed by the inner and outer walls of the inner channel. However, due to the different areas of the walls, the corresponding mean corrosion rates reach similar values at the inner walls of the inner and outer channels. For cases 2 and 3, the amount of material removed from the inner channel walls is more than two times larger than that removed from the walls of the outer channel. Results in figure 12 and table 4 show that, among the three cases studied, the least favorable conditions are predicted for the case with the lowest mass flow rate (Case 1) because of the effect of the higher temperatures and despite the lower velocities reached. Note that, in this case, the highest corrosion rates in the inner channel are reached in the entrance region to the channel, where the fluid velocity is very large, and at the end part of the channel, where the temperature is highest. In the outer channel, a large area of high corrosion rates is reached at the end part of the channel, because of the combination of high temperature and velocity values.

It can also be observed from figure 12 that the corrosion rate at the entrance of the inner channel tends to increase with the Pb–15.7Li mass flow rate through the blanket. This gives rise to the existence of a local minimum for the material removal and mean corrosion rate at both walls of the inner channel, as observed in table 4. On the other hand, the maximum and mean values of the corrosion rate and material removal in the outer channel decrease monotonically with increasing the Pb–15.7Li mass flow rate.

As mentioned before, the corrosion rate results presented above are obtained under the assumption that the corrosion process is mass-transfer controlled, which is acceptable for low enough fluid velocities. To what extent this assumption is adequate for the relatively high velocities considered in this work should be investigated [36, 39]. Another question that also needs to be analysed in the future is whether the concentrations of Fe and Cr in the Pb–Li can reach the solubility limit or not, since this situation could lead to suppression of corrosion [38]. This will require the use of a model to describe the transport of the steel elements dissolved in the flowing Pb–Li.

Besides corrosion issues, cooling efficiency and maximum allowable temperature at blanket walls are essential factors in the blanket design. Table 3 shows that the increase in the mean temperature of the Pb–15.7Li between the inlet and outlet sections of the blanket, $T_{out} - T_{in}$, which is directly related with the blanket efficiency, is below the approximate 100 °C level indicated in section 1.2.1, even for the lower mass flow rate conditions of case 1. The temperature increase predicted for cases 2 and 3, for which the predicted corrosion levels might be acceptable, are very far from the required values.

From the findings described above we deduce that the proposed blanket design requires to be modified in order to get operational scenarios that produce acceptable ranges of corrosion rates and temperature jump through the blanket. On the other hand, regarding the maximum temperature in the Pb–15.7Li, the values presented in table 3 are below the 550 °C limit mentioned in section 1.2.1, even for Case 1, so that, for the range of operational scenarios considered, the maximum Pb–15.7Li temperature does not appear to be an issue

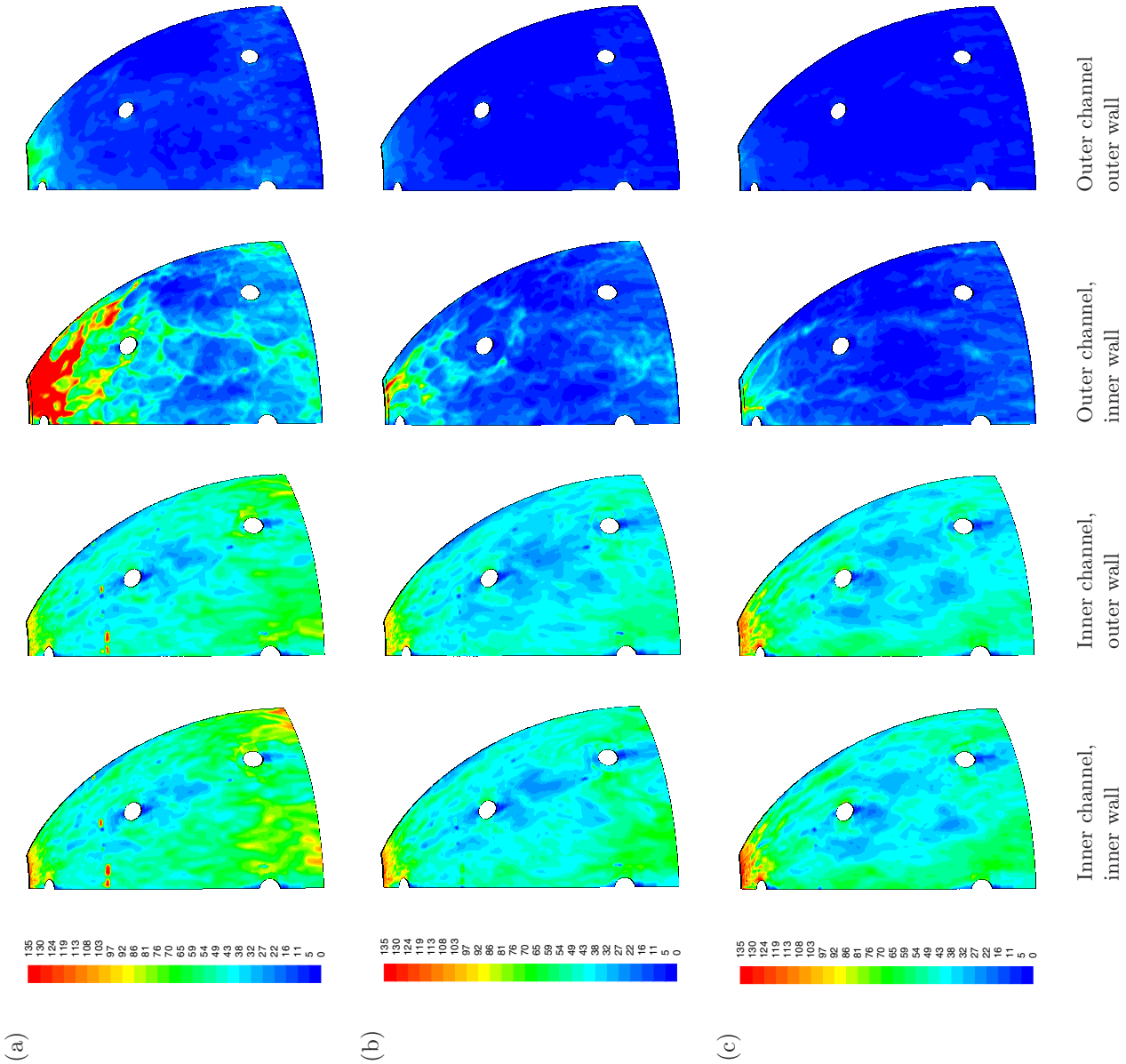

Figure 12. Corrosion rate contours (μm yr^{-1}) at the four spherical walls of the blanket module channels, for the three operational scenarios considered: (*a*) Case 1, $\dot{m}$ = 5993 kg s^{-1}; (*b*) Case 2, $\dot{m}$ = 8557 kg s^{-1}; (*c*) Case 3, $\dot{m}$ = 11 410 kg s^{-1}.

Table 3. Summary of the main results obtained from the three simulations (total released power: 82.65 MW; $T_{in} = 350$ °C).

Case	$\dot{m}$ [kg s^{-1}]	T_{max} [°C]	$T_{out} - T_{in}$ [°C]	v_{max} [μm yr^{-1}]
1	5993	520	74	330[a] (275)
2	8557	459	54	164[a] (135)
3	11 410	441	40	140[b] (105)

[a] outer channel, inner wall [b] inner channel, outer wall.

Table 4. Material removal results [cm^3 yr^{-1}] (in parenthesis, mean corrosion rate [μm yr^{-1}]).

	Inner channel		Outer channel		
Case	Inner wall	Outer wall	Inner wall	Outer wall	Total
1	1984 (66.42)	1846 (60.21)	2122 (65.70)	914.9 (23.25)	6867 (51.95)
2	1569 (52.62)	1492 (48.82)	910.0 (28.24)	546.0 (13.88)	4517 (34.17)
3	1621 (54.38)	1576 (51.58)	716.7 (22.24)	505.1 (12.84)	4419 (33.43)

(moreover, the maximum temperature values shown in table 3 are reached at very small areas).

Thus, in terms of cooling requirements, SFWB does not reach the maximum local allowable temperature imposed by the EUROFER mechanical properties. On the other hand, the temperature jump through the blanket is considerably lower than the mentioned design goal of 100 °C, so that there is still room for improvement in the design for cycle efficiency purposes. In terms of corrosion rates, the values predicted for Case 1, which exhibits the best behavior with respect to the temperature jump, are above the target of 200 μm yr^{-1}. For cases 2 and 3, however, the predicted corrosion rates fulfill the design requirements, while the temperature jump is significantly lower than 100 °C. This indicates two points:

(i) Low corrosion rates and large temperature jump for cycle efficiency exhibit a clear incompatible behavior with the mass flow rate.
(ii) Although the current SFWB design does not show yet a complete satisfactory performance, corrosion rates for the SCLL are expected to be reduced at appropriate levels by means of re-design.

4. Conclusions

The cooling of a SCLL blanket with SFWB has been studied in terms of Pb–15.7Li temperature increase through the blanket, and maximum values of the temperature and corrosion rates reached at the blanket walls. The work has been carried out by performing a numerical simulation of the deposition of neutrons energy in the Pb–15.7Li using MCNPX, and the thermo-fluid dynamics using the general purpose CFD code FLUENT with a large eddy simulation approach. The problem constitutes a difficult challenge, mainly because of the blanket geometry and dimensions, the highly turbulent Pb–15.7Li flow in the channels, and the computational resources required, related to the minimum size of the computational mesh in certain domain regions and the maximum time step required by the transient simulations. A detailed description of the Pb–15.7Li velocity and temperature distributions predicted for different operational scenarios has been presented, along with the estimated corrosion rate distribution on the blanket walls.

A relevant conclusion of this work is that the EUROFER-based SCLL scheme for IFE reactor, mainly questioned by corrosion issues, can be a viable alternative provided that a careful design of cooling ducts is considered to minimise them.

Despite the expected improvement of SFWB over the IFWB configuration, we still found an unsatisfactory behavior of the blanket from the point of view of combined cooling efficiency and corrosion levels. The maximum local temperature limit of 550 °C was not reached, as could be expected since the studied operational scenarios under study were adjusted with this criteria. On the other hand, incompatible trends were found between the desirable variations of the temperature jump through the blanket and maximum corrosion rates as a function of the mass flow rate, within ranges that did not allow us to find an appropriate value for the mass flow rate that satisfies the design goals. That is, local maximum corrosion rates below the target of 200 μm yr^{-1} are only obtained when the maximum temperature drops to about 60 °C, far from the 100 °C target requested for power cycle efficiency.

However, two positive aspects support the conclusion that the EUROFER-based SCLL is a promising proposal for HiPER or any other ICF reactor of the EUROFER-based SCLL. On one hand, the opposite trends between corrosion rates and desirable temperature jumps is highly design dependent, and could be mitigated by re-setting the Pb–15.7Li duct shapes (also taking into account beam penetrations). On the other hand, local maximum corrosion rates in the range of 200 μm yr^{-1} (expected to be significantly reduced with BB re-design) can be faced making use of anti-corrosion coatings.

Some of the drivers for future design are: (i) consolidation of SFWB configuration over IFWB. (ii) Elimination of the hemispherical modular division. (iii) Change from double channel (thin-thick) to single (thick) channel modules, and design an outlet pipe with a larger cross section area in order to prevent too large velocities in the Pb–15.7Li flow and thus excessive corrosion rates. (iv) Exploration of coatings to reduce corrosion [25].

Acknowledgments

This work has been performed within the framework of the HiPER Preparatory Phase Study European Commission-Grant Agreement 211737. The authors gratefully acknowledge the support of the funding agencies and, especially, the 'Instituto de Fusión Nuclear' and his director José Manuel Perlado, as Spanish representative and firm supporter of the Project.

This work was also supported by the Spanish MINECO (Ministerio de Economía y Competitividad) under grant AIC-A-2011-0726 to UNED within 'Programa de

internacionalización de la I+D, Subprograma relativo a infraestructuras científicas internacionales', the ETS Ingenieros Industriales-UNED grant 2014-IEN18, and the Programa de Actividades I+D de la Comunidad de Madrid under TECHNOFUSION(II)-CM (S2013/MAE-2745) Project.

References

[1] HiPER Project Team 2013 *Technical Report* No. 211737 (www.hiper-laser.org/Resources/HiPER_Preparatory_Phase_Completion_Report.pdf)
[2] Juárez R., Sanz J., Perlado J.M. and Le Garrec B. 2011 *Fusion Eng. Des.* **86** 694–8
[3] Juárez R., Sanz J. and Perlado J.M. 2012 *Fusion Eng. Des.* **87** 336–43
[4] Sanz J., Juárez R., Ognissanto F. and Perlado J.M. 2011 *Fusion Sci. Technol.* **60** 579–84
[5] Rus B. *et al* 2011 Repetition rate target and fusion chamber systems for HiPER *Proc. SPIE* **8080** 808020–9
[6] Atzeni S. *et al* 2009 *Nucl. Fusion* **49** 055008
[7] Le Garrec B. *et al* 2011 HiPER laser reference design *Proc. SPIE* **8080** 80801V–9
[8] Raffray A.R., El-Guebaly L., Federici G., Haynes D., Najmabadi F., Petti D. and ARIES-IFE Team 2004 *Fusion Sci. Technol.* **46** 417–37
[9] Álvarez J., Rivera A., González-Arrabal R., Garoz D., Del Río E. and Perlado J.M. 2011 *Fusion Sci. Technol.* **60** 565–9
[10] Juárez R., Sanz J., López-Revelles A. and Perlado J.M. 2013 *Fusion Eng. Des.* **88** 2373–7
[11] Sánchez C., Juárez R., Sanz J. and Perlado J.M. 2013 *Fusion Eng. Des.* **88** 2679–83
[12] Perlado J.M. *et al* 2011 IFE plant technology overview and contribution to HiPER proposal *Proc. SPIE* **8080** 80801Z–10
[13] Malang S., Raffray A. and Morley N. 2009 *Fusion Eng. Des.* **84** 2145–57
[14] Sardain P. *et al* 2003 *Fusion Eng. Des.* **69** 769–74
[15] Li Puma A. *et al* 2006 *Fusion Eng. Des.* **81** 469–76
[16] Malang S., Tillack M., Wong C.P.C., Morley N. and Smolentsev S. 2011 *Fusion Sci. Technol.* **60** 249–56
[17] Malang S. and Mattas R. 1995 *Fusion Eng. Des.* **27** 399–406
[18] Sawan M.E., Sviatoslavsky I.N., Raffray A.R. and Wang X. 2005 Neutronics assessment of blanket options for the HAPL laser inertial fusion energy chamber *Proc. 21st Int. Conf. on Fusion Engineering (Knoxville, TN, 26–29 September 2005)* pp 1–4 (http://web.ornl.gov/sci/fed/sofe2015)
[19] Sannier J., Dufrenoy T., Flament T. and Terlain A. 1992 *J. Nucl. Mater.* **191–4** 975–8
[20] Konys J., Krauss W., Steiner H., Novotny J. and Skrypnik A. 2011 *J. Nucl. Mater.* **417** 1191–4
[21] Flament T., Tortorelli P., Coen V. and Borgstedt H.U. 1992 *J. Nucl. Mater.* **191–4** 132–8
[22] Zinkle S.J. and Ghoniem N.M. 2011 *J. Nucl. Mater.* **417** 2–8
[23] Lindau R. *et al* 2005 *Fusion Eng. Des.* **75–9** 989–96
[24] Lässer R., Baluc N., Boutard J.L., Diegele E., Dudarev S., Gasparotto M., Möslang A., Pippan R., Riccardi B., van der Schaaf B. and van der Schaaf B. 2007 *Fusion Eng. Des.* **82** 511–20
[25] Konys J., Krauss W. and Holstein N. 2010 *Fusion Eng. Des.* **85** 2141–5
[26] Snead L., Nozawa T., Ferraris M., Katoh Y., Shinavski R. and Sawan M. 2011 *J. Nucl. Mater.* **417** 330–9
[27] CATIA V5R19 2002–2015 *Dassault Systemes* Last accessed: 2015-07-16 www.3ds.com/products-services/catia/welcome/
[28] Wu Y. 2009 *Fusion Eng. Des.* **84** 1987–92
[29] Pelowitz D.B.E. 2005 *MCNPX™ User's Manual* version 2.5.0 *Laboratory Report* LA-CP-05-0369 (Los Alamos National Library)
[30] ARIES Program *Public Information Site* Last accessed: 2015-07-16 http://aries.ucsd.edu/ARIES/WDOCS/ARIES-IFE/SPECTRA/
[31] Santamarina A. *et al* 2009 JEFF Report 22. Validation results from JEF-2.2 to JEFF-3.1.1 *Technical Report* No. 6807 Nuclear Energy Agency (NEA)
[32] FLUENT 2006 *User's Guide* ver 6.3 (USA: Fluent)
[33] Jauch U., Haase G. and Schulz B. 1986 Thermophysical properties in the system Li-Pb, part II: thermophysical properties of Li(17)Pb(83) eutectic alloy *Report* KfK 4144 (Kernforschungszentrum, Karlsruhe)
[34] Germano M., Piomelli U., Moin P. and Cabot W.H. 1991 *Phys. Fluids* **3** 1760–5
[35] Lilly D.K. 1992 *Phys. Fluids* **4** 633–5
[36] Balbaud-Célérier F. and Barbier F. 2001 *J. Nucl. Mater.* **289** 227–42
[37] Kondo M., Takahashi M., Suzuki T., Ishikawa K., Hata K., Qiu S. and Sekimoto H. 2005 *J. Nucl. Mater.* **343** 349–59
[38] Kondo M., Takahashi M., Tanaka T., Tsisar V. and Muroga T. 2012 *Fusion Eng. Des.* **87** 1777–87
[39] Smolentsev S., Saedi S., Malang S. and Abdou M. 2013 *J. Nucl. Mater.* **432** 294–304
[40] Sannier J., Flament T. and Terlain A. 1991 Corrosion of martensitic steels in flowing Pb17Li *Fusion Technology* ed B.E. Keen *et al* (New York: North-Holland) pp 901–5